

The ASDEX Upgrade Divertor IIb – a Closed Divertor for Strongly Shaped Plasmas

R. Neu, T. Eich, J.C. Fuchs, A. Kallenbach, C. Maggi, V. Rohde, F. Ryter, J. Gafert, O. Gruber, G. Haas, A. Herrmann, M. Kaufmann, M. Laux, V. Mertens, H.W. Müller, J. Neuhauser, T. Pütterich, J. Stober, S.W. Yoon and the ASDEX Upgrade Team

Max-Planck-Institut für Plasmaphysik, EURATOM Association, D-85748 Garching, Germany

e-mail contact of main author: Rudolf.Neu@ipp.mpg.de

Abstract. A new divertor configuration (DIV IIb) has been implemented in ASDEX Upgrade. In order to accommodate a large variety of plasma shapes with bottom triangularities (δ_{bot}) up to 0.48, the outer strike point region was modified and the roof baffle was lowered and diminished at its outer part in comparison with the previous divertor (DIV II). The inner part of the divertor strike point module remains unchanged, but at the divertor entrance a smooth transition to the central column is provided to minimize local hydrogen recycling. The beneficial behaviour of DIV II is essentially maintained. There is an increase of the power density due to geometrical reasons at the outer target, whereas the divertor radiation for similar configurations and discharge conditions is unchanged. The pumping characteristics for D and He are almost retained, suggesting a large influence of the inner divertor leg, the configuration of which remains as before. A significant reduction (20 %) of the L-H threshold is observed consistent with larger temperature gradients inside the separatrix just before the transition.

1. Introduction

In 1997 the original "open" ASDEX Upgrade Divertor I (DIV I) was replaced by the rather "closed" LYRA-Divertor (DIV II) [1]. In support of ITER, DIV II (Fig. 1, shaded divertor structure) had been designed for low target power load, optimal divertor radiation losses and high pumping efficiency, if used in connection with a narrow class of well-fitting low δ equilibria. These expectations were confirmed during a run period of several years [1,2]. In parallel with these optimized divertor studies, increasing interest developed in strongly shaped plasmas, because of their improved confinement at high plasma densities and the access to type-II ELMs [3]. High δ plasmas could only be produced in the DIV II geometry by positioning the outer divertor plasma leg on the top of the roof baffle located between the two curved vertical targets. In these kind of discharges some of the DIV II benefits were therefore degraded, especially the power load characteristics at the outer strike point. Additionally, the pumping capability of the cryo-pump was also lower for this kind of discharges.

To overcome this, the roof baffle and the outer part of the divertor were redesigned (Fig. 1, dark divertor structure) to accommodate a large variety of plasma shapes with bottom triangularities up to 0.48. As a result of the positive experience of power handling in DIV II, ordinary fine grain graphite has been chosen for the outer strike point region in DIV IIb [4]. The tiles are slightly tilted in toroidal direction (as they were in DIV II) in order to protect the edges. Since

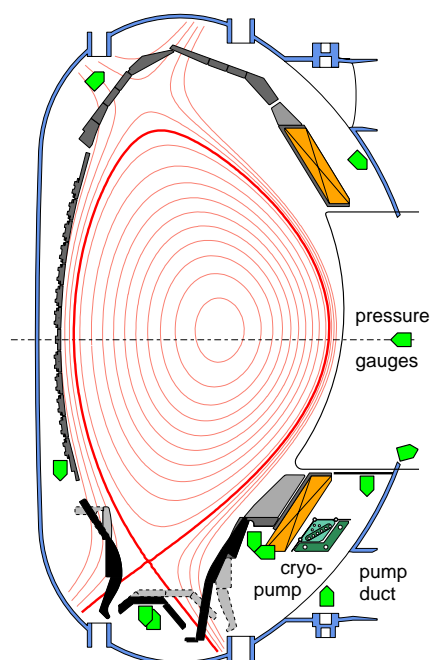


Fig. 1: Poloidal cross section of ASDEX Upgrade showing DIV II (shaded) and the new DIV IIb as well as the upper divertor with high δ lower single null plasma equilibrium.

the poloidal cross section of the outer strike point module is flat and not curved anymore the angle between the flux surfaces in the strike zone vicinity is increased by a factor of about 2 compared to DIV II [5]. At the inner part of the divertor, a smooth transition from the central column to the divertor entrance is provided to minimize hydrogen recycling. The strike point module itself remains unchanged compared to DIV II. The roof baffle is lowered and its width is reduced to allow the outer divertor plasma leg to hit the strike point module even for $\delta \approx 0.5$. The new geometry of DIV I Ib was chosen in such a way, that the distance of the strike points to the pumping gaps is lowest for medium δ equilibria. The conductance to the cryo-pump is not affected by the mechanical changes and due to the simpler shape of the outer strike point module, the diagnostic access is substantially facilitated. More details on the design of DIV I Ib can be found in [4].

Since spring 2001, ASDEX Upgrade has been successfully operated with DIV I Ib and discharges with additional heating powers up to 18 MW have already been performed.

2. Power Deposition

Due to the larger angle between the strike point module and the flux surfaces in DIV I Ib, the

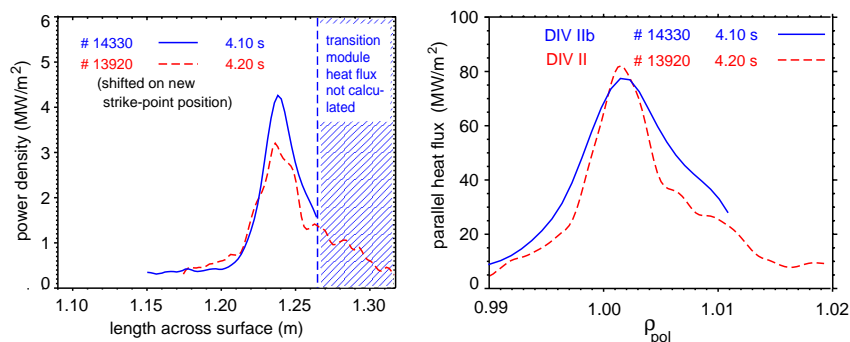


Fig. 2: Power density (left) and parallel heat flux (right) at the outer strike point in DIV I Ib (#14330, $\bar{n}_e \approx 6.6 \cdot 10^{19} m^{-3}$, solid line) and DIV II (#13920, $\bar{n}_e \approx 5.1 \cdot 10^{19} m^{-3}$, dashed line) during a 5MW NBI-heated H-Mode discharge.

wetted area is smaller and narrower profiles with a higher peak power density are expected compared to DIV II. Indeed thermographic measurements showed that the maximum power density at the target is 50% higher compared with DIV II for otherwise comparable H-Mode discharges (Fig.2). Since the power load in DIV II was very low even for the highest heating power [2] this increase is tolerable even using graphite instead of CFC (see also Fig.2). The routine operation near double null offers also the possibility for investigations of power deposition characteristics when changing to an upper null configuration. As known from lower single null experiments with ∇B away from the x-point a more symmetric peak power depositions is reached in the upper single null configuration. The new fast thermography system ($\tau_{frame} = 200\mu s$) for the upper divertor allows also the measurement of the ELM dynamics. Code simulations for the different power load profiles have recently initiated and systematic investigations on the role of the magnetic field direction will be performed in the next campaign.

3. Divertor Radiation

Divertor radiation plays a crucial role in dispersing spatially the power flowing parallel to the flux tubes towards the divertor strike zones. The strong reduction of the power load due to high divertor radiation observed in DIV II [2] was also found in DIV I Ib as already reported in [6]. Beside this average behaviour a rather large scatter of the ratio of the main chamber/divertor radiation is observed which lies outside the errors of the measurements. Although the reason for this observation is not yet clear it might support the picture of self adjusting divertor radiation:

For strong main chamber radiation less power reaches the divertor leading to less C-erosion and radiation, and vice versa. Detailed investigations of the divertor radiation profiles were performed by increasing the spatial resolution using the plasma shift technique [7]. There, a radiation maximum very close to the strikepoint is observed, which gets broader for higher neutral densities and even departs from the strikepoint as the plasma detaches and finally a MARFE is formed. The species of the main plasma gas (H, D or He) has also an influence on the radiation distribution. In the outer divertor the radiation levels are similar for all species, but the radiation profiles in front of the strike points are located differently. In D the maximum of the profile is nearest to the strikepoint position, whereas it is shifted away in H and even more in He-discharges. As can be judged from Fig. 3, the shape of the total radiation profile is very similar to the deconvoluted profile of the C III emission [7], which again suggests that the total divertor radiation is dominated by carbon, at least in the case of deuterium discharges. The further investigation of the obviously important role of carbon radiation in the divertor will be one of the key issues when proceeding with the the elimination of C-surfaces in the course of the W-programme [8] at ASDEX Upgrade.

4. Detachment characteristics

Detachment and the density limit were investigated in dedicated H and D L-Mode density limit discharges and compared to earlier experiments in ASDEX Upgrade (DIV I) and in JET (MK IIA) [9]. The data could be fitted reasonably well within the model described in [10] which uses a two-point model and Bohm-like perpendicular transport to connect the upstream plasma parameters to the divertor. As a result of the fit to the model a very weak isotope dependence ($m^{0.1}$) and a size dependence proportional to $R^{-0.36}$ is found for the density limit. One can use the extracted scaling to calculate the density for the onset of detachment in an ITER L-Mode discharge taking the nominal ITER parameters and assuming a net power of 30 MW flowing over the separatrix. This leads to a similar main chamber density where the detachment occurs as in ASDEX Upgrade, pointing to a reasonable operational space for non-burning ITER plasmas.

5. Hydrogen and Helium Pumping

Neutral flux densities Γ_0 are measured by ionisation gauges at different locations in the vacuum vessel (see Fig. 1). In the DIV II configuration, the 'natural' H-Mode density was significantly higher for high- δ discharges compared to low- δ discharges (factor of ≈ 1.5 , depending on auxiliary heating power). This was partly attributed to a decreased pumping capacity due to the unfavourable positioning of the outer divertor plasma leg on the roof baffle, causing a lower Γ_0 in the private flux region PFR. However, Γ_0 appears very similar for both versions of the divertor for low- δ as well as for high- δ discharges. These observations were somewhat unexpected since in DIV IIb the outer strike point position is less favourable for low- δ discharges and more favourable for high- δ discharges compared to DIV II, but they are consistent with most recent simulations using the B2-Eirene code [11]. It might be explained by the fact that the divertor neutral pressure is mainly determined by the colder inner divertor leg, the configuration of which remained unchanged, and that the plugging by the outer leg is still effective

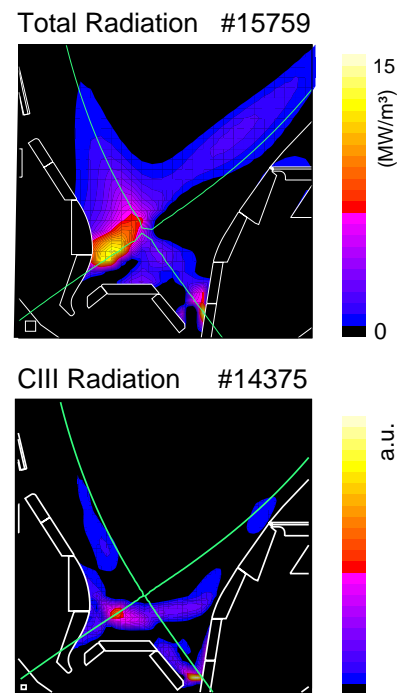


Fig. 3: Profiles of radiation and CIII emissivities for similar D-discharges ($I_p = 1$ MA, $B_t = 2.5$ T, $\bar{n}_e = 9 \cdot 10^{20} \text{ m}^{-3}$, $\delta = 0.37$)

despite its large distance to the outer divertor gap in low- δ discharges. In high- δ discharges, the lower Γ_0 in the PFR for a given plasma density could be caused by a generally increased particle confinement in parallel to the increased energy confinement as described in [12]. Dedicated experiments were performed to investigate the influence the divertor bypasses on the effective exhaust rate in DIV I Ib and on the main chamber recycling. They are described in detail in [6,13]. A key feature of DIV II was the high He compression ($C_{He} = n_{He,0}^{div}/n_{He,+}^{core}$) accomplished by the narrow divertor channel which hindered efficiently the back flow of neutral He into the main chamber. The He compression in DIV I Ib was evaluated from the He exhaust time constant via a three chamber model [14]. Fig. 4 shows a comparison of the He compression in DIV II [14] and DIV I Ib as a function of the neutral flux density below the roof baffle. The data in DIV II (open symbols) were all taken at low triangularity, whereas the data of DIV I Ib comprise low and high- δ discharges (see legend Fig. 4). No significant difference between both divertors is found at low triangularities. At higher triangularities the He compression is lower by about a factor of 2-3 for similar heating powers.

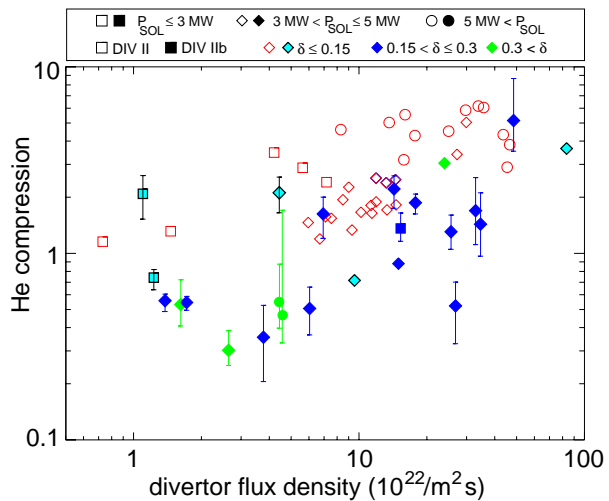


Fig. 4: He compression as a function of Γ_0 . Full symbols represent data from DIV I Ib, their shape the heating power and their colour δ . DIV II measurements are only taken at $\delta \approx 0.15$. The 'error'-bars indicate the scatter of the He compression when evaluated from different spectroscopic observations.

6. Divertor Effect on the H-mode Threshold

In order to monitor the conditioning of the machine as well as to obtain a measure for the 'natural' scatter of threshold and confinement data, a 'standard' H-Mode discharge ($I_p = 1$ MA, $B_t = 2$ T, $q \approx 3.2$, $\delta \approx 0.15$) has been performed routinely since 1999 each day of operation [15]. Comparing the L-H transition power threshold a clear reduction of about 20% is found for DIV I Ib compared to DIV II [6]. Using a combination of edge Thomson scattering and lithium beam measurements, both the edge plasma parameters and the actual separatrix position can be extracted very precisely [16]. These measurements indicate that right before the L-H transition, the density at the separatrix position and slightly inside is very similar for both divertors. This is true also for the electron temperature at the separatrix, which is around 50 eV. However, the temperature gradient inside the separatrix is significantly larger with the new divertor, pointing out the importance of local edge parameters, as already seen after the change from DIV I to DIV II, where an increase of the threshold was found [1]. As can be judged from Fig. 5, there is obviously a weaker density dependence of the threshold as found for the former divertor configurations and as predicted by the scaling ($P_{thresh} \sim \bar{n}_e^{0.46} B_t^{0.87}$) [17]. Additionally, an increase of the threshold with the triangularity seems to appear. At present it is not totally clear whether these observations are influenced by the simultaneously installed tungsten coated central column [8] by leading to a change in the edge radiation.

7. Parasitic Sub-Divertor Plasma

The interesting feature of a sub-divertor plasma has been revealed by the recent installation of a Langmuir probe below the roof baffle [18]. Typically, electron temperatures in the range of 10 eV were measured under attached divertor conditions, decreasing to values below 5 eV after detachment. The densities can vary by three orders of magnitudes up to $n_e = 10^{18} \text{ m}^{-3}$. Since

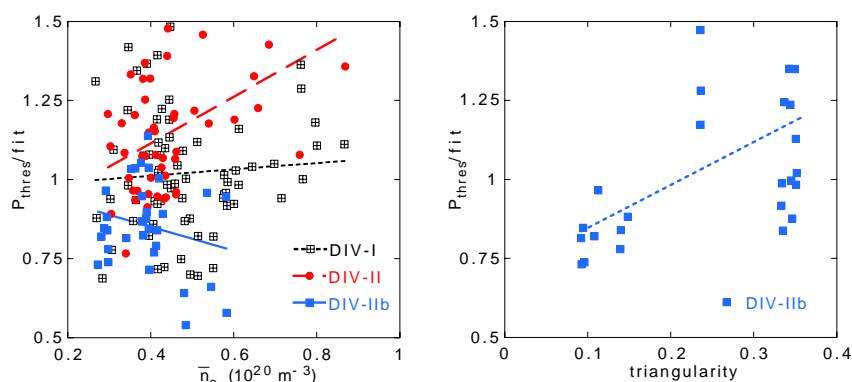


Fig. 5: H-Mode threshold normalized to the scaling deduced in [17] as a function of density for $\delta \approx 0.15$ deuterium discharges (left). Normalized H-Mode threshold as a function of δ in DIV IIb.

the probe is not connected via magnetic field lines to the main divertor plasma, the plasma must be created underneath the divertor structure itself. Geometrical considerations lead to a very short loss time in the order of $\tau_{loss} \approx 100 \mu s$, meaning that the plasma must be produced very effectively at the same field line, which hits the probe position. In a regression analysis for the density of the parasitic plasma a strong dependence on the divertor radiation and the neutral flux is found ($n_e^{div} \sim P_{rad,div}^{2.7} * \Gamma_0^{0.7}$) [18]. This leads to hypothesis that the plasma is created by photo-effect on (metallic) surfaces or photo-ionisation of C_xH_y or D. Using the argument of power balance between the input by radiation and the loss by ionisation for a qualitative estimate one can at least show that the process is feasible: Taking $N_e = 10^{17}$ particles, $T_e = 10$ eV and $\tau_{loss} \approx 100 \mu s$ as typical parameters an absorbed power in the order of a few kW is sufficient. The existence of a plasma below the divertor may have direct consequences for the deposition of C_xH_y species, which has a strong impact on the hydrogen (reactor: tritium) inventory of a device. On their way to the pumps hydrocarbon molecules have to cross the parasitic plasma, resulting in ionisation of the species. This may lead to the deposition of hard a-C:H layers with short spatial decay lengths, as observed in [18].

References

- [1] H.S. BOSCH et al., *Plasma Phys. Controlled Fusion* 41, A401 (1999).
- [2] A. KALLENBACH et al., *Nucl. Fusion* 39, 901 (1999).
- [3] J. STOBER et al., *Nucl. Fusion* 41, 1123 (2001), and ref. therein.
- [4] O. GRUBER et al., *Technical Report 1/322*, IPP, Garching, Germany, 1999.
- [5] A. HERRMANN et al., *Plasma Phys. Controlled Fusion* 44, 883 (2002).
- [6] R. NEU et al., *Plasma Phys. Controlled Fusion* 44, 1021 (2002).
- [7] J.C. FUCHS et al., 29th EPS Conf. on PPCF, Montreux, ECA Vol. 26B (2002) P-1.047.
- [8] V. ROHDE et al., this conference, EX/D1-4
- [9] C. MAGGI et al., Proc. 29th EPS Conf. on PPCF, Montreux, ECA Vol. 26B (2002) P-1.046.
- [10] C. MAGGI et al., *Nucl. Fusion* 39, 979 (1999).
- [11] D. COSTER et al., *Plasma Phys. Controlled Fusion* 44, 979 (2002).
- [12] O. GRUBER et al., *Nucl. Fusion* 41, 1369 (2001).
- [13] A. KALLENBACH et al., this conference, EX/P4-05.
- [14] H.S. BOSCH et al., *J. Nucl. Mater.* 290–293, 836 (2001).
- [15] F. RYTER et al., *Plasma Phys. Controlled Fusion* 44, A407 (2002).
- [16] J. NEUHAUSER et al., *Plasma Phys. Controlled Fusion* 44, 855 (2002).
- [17] J. SNIPES et al., this conference, CT/P-04.
- [18] V. ROHDE et al., accepted for publication in *J. Nucl. Mater.*